

# Randomness in atomic disorder and consequent squandering of spin-polarization in a ferromagnetically fragile quaternary Heusler alloy FeRuCrSi

Shuvankar Gupta<sup>1,\*</sup>, Sudip Chakraborty<sup>1</sup>, Vidha Bhasin<sup>2</sup>, Celine Barreateau<sup>3</sup>, Jean-Claude Crivello<sup>3,4</sup>, Jean-Marc Greneche<sup>5</sup>, S.N. Jha<sup>6</sup>, D. Bhattacharyya<sup>2</sup>, Eric Alleno<sup>3</sup>, and Chandan Mazumdar<sup>1†</sup>  
<sup>1</sup>Condensed Matter Physics Division, Saha Institute of Nuclear Physics, 1/AF, Bidhannagar, Kolkata 700064, India  
<sup>2</sup>Atomic & Molecular Physics Division, Bhabha Atomic Research Centre, Mumbai 400 094, India  
<sup>3</sup>Univ Paris Est Creteil, CNRS, ICMPE, UMR 7182, 2 rue H. Dumant, 94320 Thiais, France  
<sup>4</sup>CNRS-Saint-Gobain-NIMS, IRL 3629, Laboratory for Innovative Key Materials and Structures (LINK), 1-1 Namiki, 305-0044 Tsukuba, Japan  
<sup>5</sup>Institut des Molécules et Matériaux du Mans, IMMM, UMR CNRS 6283, Le Mans Université, Avenue Olivier Messiaen, Le Mans Cedex 9, 72085, France and  
<sup>6</sup>Beamline Development and Application Section Physics Group, Bhabha Atomic Research Centre, Mumbai 400085, India  
(Dated: June 7, 2024)

$\text{Ru}_{2-x}\text{Fe}_x\text{CrSi}$  ( $0 < x < 1$ ) system is theoretically predicted to be one of the very few known examples of robust half-metallic ferromagnet with 100% spin polarization. Since Cr is considered to be the main contributor to magnetism, the Fe/Ru substitution is not expected to disturb its magnetic properties any significantly, and hence all Fe-containing members of the series are predicted to follow Slater-Pauling rule with a saturation magnetic moment of  $2 \mu_B/\text{f.u.}$  However, contrarily to the theoretical expectations, some experiments rather show a linear variation of the saturation magnetization and Curie temperature with Fe ( $x$ ) substitution. The equiatomic member FeRuCrSi of this family is also considered as a technologically important material, where the band structure calculations suggest the material to be spin gapless semiconductor. Through our in-depth structural analysis of FeRuCrSi using X-ray diffraction, extended X-ray absorption fine structure and <sup>57</sup>Fe Mössbauer spectrometry, we found a random disorder between Fe and Ru sites, while the magnetic moment in this system is actually contributed by Fe atoms, questioning the very basic foundation of the half-metallic character proposed by all theoretical calculations on  $\text{Ru}_{2-x}\text{Fe}_x\text{CrSi}$  series. Our Mössbauer result also envisions a rather rare scenario where the main physical properties are intricately correlated to the chemistry of the material in the form of random atomic disorder on a localised scale.

## I. INTRODUCTION

Spintronics has emerged as a promising field in nano-electronics, offering the potential for more efficient and powerful devices by mitigating power consumption while enhancing memory and processing capabilities [1–3]. A critical aspect of spintronics is the exploration of materials with high spin-polarization, deemed ideal for advancing spintronic technologies [4]. Particularly, half-metallic ferromagnets (HMFs) [5] and spin gapless semiconductors (SGSs) [6] are recognized for their high spin polarization and versatile magnetic properties, making them valuable for enhancing the efficiency of spintronic devices across various applications such as spin valves [7], data storage, magnetic sensors [4], spin injectors [8], and magnetic tunnel junctions [9].

Heusler alloys have recently garnered attention due to their diverse properties, including half-metallicity [10–14], spin gapless semiconductivity [15–17], spin-semimetals [18, 19], spin glass [20], re-entrant spin glass [21], bipolar magnetic semiconducting characteristics [22], *etc.* The exploration of new Heusler alloys is crucial for advancing this area of study, as despite theoretical predictions [23–26] of numerous Heusler alloys

possessing SGS features, only a limited number of experimental realizations have been achieved so far [15–17, 27]. Among them,  $\text{Mn}_2\text{CoAl}$  [27],  $\text{CoFeMnSi}$  [15],  $\text{CoFeCrGa}$  [16], and  $\text{CoFeMnSn}$  [17] have been experimentally established as SGS materials, with the additional discovery of fully compensated ferrimagnetic SGS in  $\text{CrVTiAl}$  [28]. It is pertinent to note here that the most of the Heusler alloys often form with inherent and irrepressible structural disorder which is generally argued to be responsible for the nonconformity with the theoretically predicted HMF and SGS properties. So, finding compound having robust HMF and SGS properties will be an effective solution for this kind of situation.

$\text{Ru}_{2-x}\text{Fe}_x\text{CrSi}$  is one such system where first principles band structure calculations predict robust HMF properties against structural disorder throughout the series [29–31]. The equiatomic member of the series, FeRuCrSi, has been additionally predicted to exhibit SGS characteristics [32–34]. The quaternary compound FeRuCrSi can be thought of as the intermediate between two ternary Heusler alloys  $\text{Fe}_2\text{CrSi}$  [35] and  $\text{Ru}_2\text{CrSi}$  [36]. Since Ru and Fe are isoelectronic atoms, the total valence electron count (VEC) of all members of  $\text{Ru}_{2-x}\text{Fe}_x\text{CrSi}$  remain invariant (VEC = 26) irrespective to the value of  $x$ . Following the Slater-Pauling (S-P) rule [37, 38] for HMF Heusler alloy, the total magnetic moment for any member of the series is expected to be  $M = (\text{VEC} - 24) = 2 \mu_B/\text{f.u.}$  However, the Ru-rich end-composition,  $\text{Ru}_2\text{CrSi}$  is exper-

\* guptashuvankar5@gmail.com

† chandan.mazumdar@saha.ac.in

imentally found to undergo antiferromagnetic transition below  $T_N \sim 14$  K [36]. Subsequent theoretical calculation indeed shows lower ground state energy for the antiferromagnetic spin arrangement in this compound [39]. As Fe concentration is gradually increased, the system initially transforms to a spin-glass state, before it finally settles to a ferromagnetic ground state for  $x > 0.3$  [31, 40–43].  $\text{Fe}_2\text{CrSi}$ , the other-end member of the series, exhibit Curie temperature at 520 K with saturation magnetic moment of  $2 \mu_B/\text{f.u.}$ , in line with the S-P rule [35]. Theoretical calculations suggests Cr-atoms are the major contributor of magnetism in this series of compounds, although this postulation is yet to be experimentally verified for compositions with  $x \neq 0$ . Interestingly, some of the experimental reports rather suggest that a linear variation of magnetic moment occur with Fe substitution in  $\text{Ru}_{2-x}\text{Fe}_x\text{CrSi}$ , contrary to the invariance of magnetic moment expected from the S-P rule for HMF systems [40]. Additionally, even for  $\text{FeRuCrSi}$ , large variations in its basic properties like Curie temperature ( $T_C$ ) and saturation magnetization ( $M_{sat}$ ) at low temperature have been reported in the literature [33, 40]. Thus, the members of  $\text{Ru}_{2-x}\text{Fe}_x\text{CrSi}$  series not only sometimes fail to conform to the theoretical prediction, the experimental results on  $T_C$  and  $M_{sat}$  reported by different groups on the same compositions are also not reproducible. As mentioned earlier, since the Heusler alloys are known to form with inherent structural disorder, *a priori* one would expect that such variations in properties reported by various groups are related to different natures and extents of disorder present in the respective materials, despite having the same nominal composition. In this work, we have focussed on the equiatomic  $\text{FeRuCrSi}$ , and investigated the nature of disorders to explain the above-mentioned discrepancies among different experimental results as well as between experiment and theory. Very surprisingly, our investigation reveals that completely contrary to the theoretically established magnetic moment on Cr in  $\text{FeRuCrSi}$ , the magnetism is actually contributed by Fe atoms. The large variation in  $T_C$  and  $M_{sat}$  can also be explained by the local arrangement of Fe/Ru in each unit cells. Our work thus firmly establishes not only the role of anti-site disorders, but the effect of randomness of Fe/Ru distribution in this compound as well.

## II. METHODS

### A. Experimental

The polycrystalline  $\text{FeRuCrSi}$  compound was synthesized via arc melting, employing high-purity constituent elements (purity  $> 99.99\%$ ) under the argon atmosphere. The synthesis process involved 5-6 melting cycles, with flipping the sample between each cycle to ensure composition homogeneity. A part of the sample was annealed for 5 days at 1073 K, followed by a quench in an ice-water mixture. Room temperature powder X-ray diffrac-

TABLE I. Calculated enthalpy of formation ( $\Delta_f H$ ) for 3 different ordered atomic arrangement of  $\text{FeRuCrSi}$ .

	4a	4b	4c	4d	$\Delta_f H$ (kJ/mol by atoms)
Type-1	Si	Cr	Ru	Fe	-33.63
Type-2	Si	Ru	Cr	Fe	-4.04
Type-3	Si	Fe	Cr	Ru	-29.25

tion (XRD) analysis was performed using  $\text{Cu-K}\alpha$  radiation on a TTRAX-III diffractometer (Rigaku, Japan). The single-phase composition and crystal structure of the sample were determined through Rietveld refinement using the FULLPROF software package [44].

Extended X-ray absorption fine structure (EXAFS) measurements were conducted at the Energy Scanning EXAFS beamline (BL-9) at the Raja Ramanna Centre for Advanced Technology (RRCAT) in Indore, India, employing standard EXAFS measurement protocols [13, 21]. Magnetic measurements were carried out in the temperature range of 3–380 K under magnetic fields up to 70 kOe using a commercial SQUID-VSM instrument (Quantum Design Inc., USA).  $^{57}\text{Fe}$  transmission Mössbauer spectrometry was conducted at both room temperature (300 K) and liquid nitrogen temperature (77 K) to investigate the local atomic environments of Fe atoms in the sample. The samples consisted of a thin powder layer containing about 5 mg  $\text{Fe}/\text{cm}^2$ . Spectra were collected using an electromagnetic transducer with a triangular velocity profile and a  $^{57}\text{Co}$  source diffused into a Rh matrix within a bath cryostat. The hyperfine structures were modeled using a least-square fitting procedure, involving quadrupolar doublets composed of Lorentzian lines, utilizing the in-house program ‘MOSFIT’. Isomer shift values were reported with reference to  $\alpha\text{-Fe}$  at 300 K, and the velocity was controlled using a standard of  $\alpha\text{-Fe}$  foil.

### B. Computational

The enthalpy of formation, electronic structure, and spin polarization at ground state were determined using Density Functional Theory (DFT) calculations with the projector augmented wave (PAW) method [45], as implemented in the Vienna ab initio simulation package (VASP) [46, 47]. The exchange-correlation was modeled by the generalized gradient approximation modified by Perdew, Burke, and Ernzerhof (GGA-PBE) [48]. Detailed information on calculation parameters can be found in previous literatures [12–14, 21].

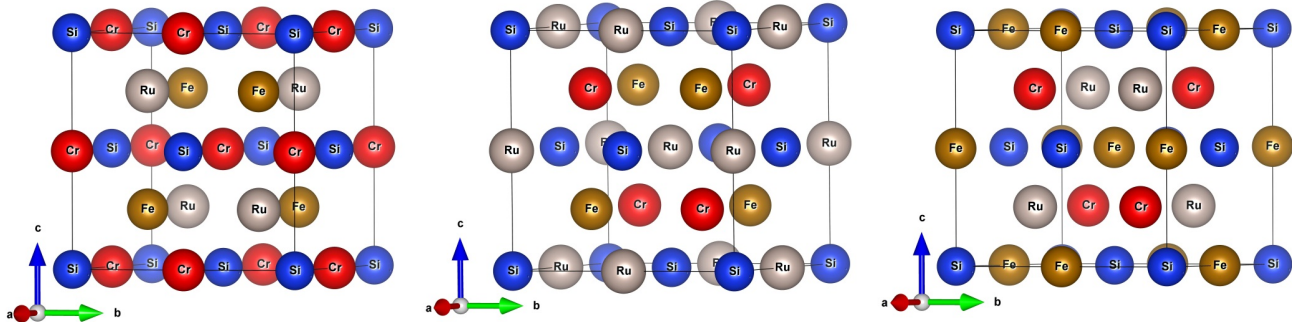


FIG. 1. Atomic arrangements of FeRuCrSi for (a) Type-1 (b) Type-2 (c) and Type-3 structure.

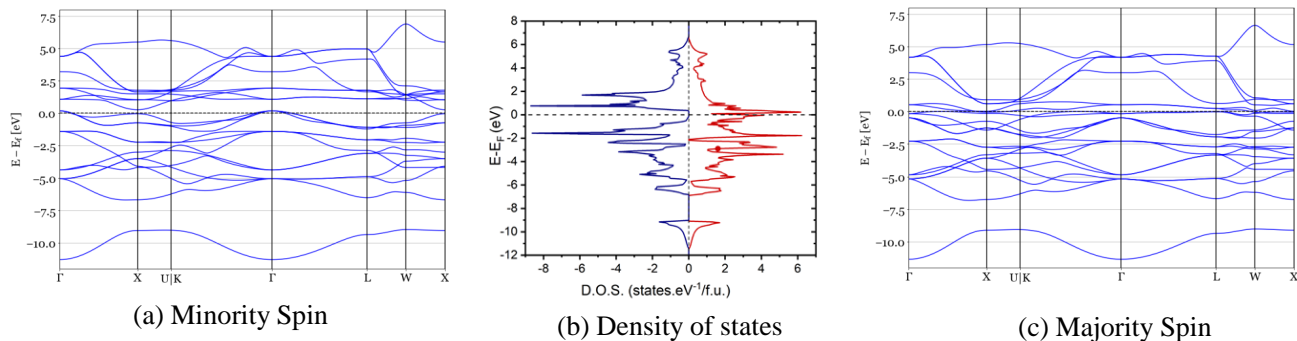


FIG. 2. Spin-polarized band structure and density of states of FeRuCrSi in ordered Type-1 structure: (a) minority spin band (b) density of states, (c) majority spin band.

### III. RESULTS AND DISCUSSION

#### A. Structure optimization and electronic structure calculations

A quaternary Heusler alloy, denoted as  $XX'YZ$ , possesses four distinct crystallographic sites:  $4a$  (0,0,0),  $4b$  (0.5,0.5,0.5),  $4c$  (0.25,0.25,0.25), and  $4d$  (0.75,0.75,0.75). Generally, the  $sp$ -element  $Z$  occupies the  $4a$  position, while the transition metals reside in the remaining three sites. Although there are six possible configurations, permutations of atoms in the  $4c$  and  $4d$  positions result in energetically equivalent configurations. Consequently, only three distinct configurations (Type-1, 2, and 3) were considered, as presented in Fig. 1 and Table I. The relative stabilities of these configurations were assessed through DFT calculations by comparing their enthalpies of formation.

Our DFT calculations on the ordered structure revealed that Type-1 configuration, with Si at  $4a$ , Cr at  $4b$ , Ru at  $4c$ , and Fe at the  $4d$  position, is the most stable. The spin-polarized band structure and density of states (DOS) for the Type-1 configuration are depicted in Fig. 2. The DOS illustrates a band gap at the Fermi level ( $E_F$ ) for the spin-down band, indicative of a metallic character for the spin-up band. This unique band structure characterizes the material as a Half-Metallic Ferromagnetic

(HMF) compound, as affirmed by a very high polarization of  $P = \frac{\text{DOS}^+(\text{E}_F) - \text{DOS}^-(\text{E}_F)}{\text{DOS}^+(\text{E}_F) + \text{DOS}^-(\text{E}_F)} = 100\%$ . Our result thus matches well with the theoretically calculated DOS on the same compound predicting the HMF character [34], although some other studies additionally predicted SGS characteristics as well [32, 33].

Consistent to that expected for HMF systems with VEC 26 [37, 38, 49], our calculation also yields the magnetic moment to be  $1.943 \mu_B$ . Moreover, atom-specific magnetic moments were computed, revealing values of Fe =  $0.146 \mu_B$ , Ru =  $-0.18 \mu_B$ , Cr =  $1.984 \mu_B$ , and Si =  $-0.007 \mu_B$  for the ordered structure, conforming with earlier published reports [32–34]. The theoretical analysis suggests that Cr significantly contributes to the magnetic moment, and the moment on the Fe site rather exhibits an induced character. Similar behaviour has earlier been observed in FeMnVA1 [12] and FeMnVGa [13] where magnetic atom Mn and nonmagnetic Fe are distributed randomly in the  $4c$  and  $4d$  sites, although in FeRuCrSi, Cr occupies  $4b$  sites whereas Ru and Fe occupy  $4c$  and  $4d$  positions, respectively.

#### B. X-ray diffraction

We have carried out XRD measurements at room temperature for both as-cast as well as annealed sample. We

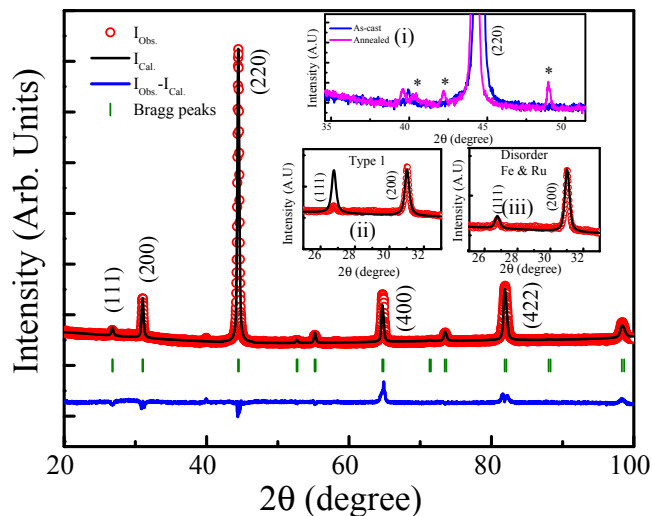


FIG. 3. Rietveld refinement of the powder XRD pattern of FeRuCrSi (disordered structure) measured at room temperature. Inset (i) shows the magnified view of the XRD data for as-cast and annealed compound, where the impurity peaks in the annealed sample are marked by asterisk sign. Inset (ii) and (iii) show the magnified view of the Rietveld refinement results considering the ordered structure and disordered structure, respectively.

found a few additional small peaks in the XRD patterns of the annealed sample which are absent in the XRD pattern of the as cast samples and also not conforming to the cubic character of Heusler alloy (inset (i) of Fig. 3). The result thus suggest that annealing tend to introduce secondary phase in the system. Consequently, all further measurements are carried out on as-cast compound only. Fig. 3 represent the Rietveld refinement of the XRD pattern of as-cast FeRuCrSi. Theoretical calculations suggests that ordered Type-1 structure possess minimum energy compared to other ordered structures. However, the earlier published experimental results on the crystal structure of FeRuCrSi are quite contradictory. Although some of the reports suggested the ordered LiMgPdSn structure-type [40], a few others also reported disordered atomic arrangements without determining the exact nature of disorder [33].

Our attempt to fit the XRD pattern using the ordered Type-1 structure model however failed to properly address the superlattice (111) Bragg peak intensity (inset (ii) of Fig. 3). For Heusler systems, the (111) and (200) Bragg peak intensities are considered to be indicative of structural disorder present in the system. For example, in *A2*-type (random mixing of elements in *4a*, *4b*, *4c* and *4d* sites) disorder, both the peaks found to be absent whereas in *B2*-type (cross-substitution between *4a* & *4b* and between *4c* & *4d*) only the (111) peak vanishes. In our case, both the 111 and 200 lines are present, thus ruling out *A2* and *B2*-type disorder (inset (iii) of Fig. 3). Nonetheless, the intensity of 111 line is substantially reduced when compared to the theoretically estimated one for an ordered Type-1 structure. The reduction in in-

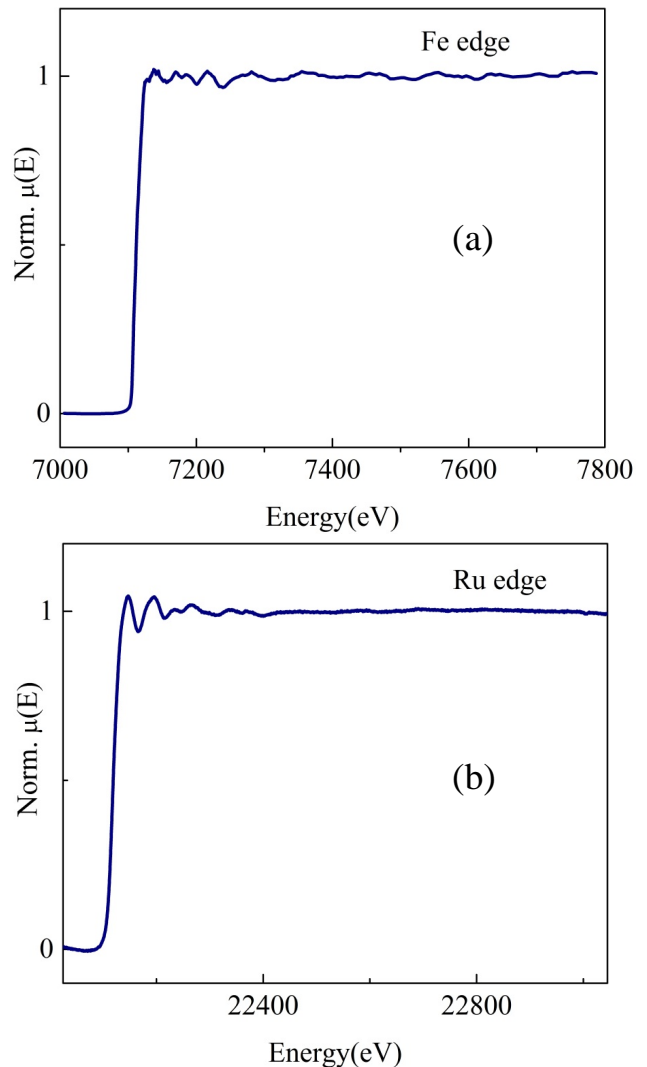


FIG. 4. Normalized EXAFS spectra of FeRuCrSi taken at (a) Fe edge and (b) Ru edge

tensity of (111) peak, however, could be accounted for if the disorder is limited to the *4c* and *4d* sites only, where Fe and Ru atoms are distributed in 50:50 ratio, averaging over the sample volume. This type of disorder earlier observed in CoRuMnSi [50], FeMnVAl [12], FeMnVGa [13] and NiRuMnSn [21]. Since the x-ray scattering cross-section of Cr and Fe are very similar, XRD remains insensitive to any further disorder between Cr (*4b*) and Fe (*4c/4d*) sites. The lattice parameter is found to be 5.757 Å, and matches with most of the other reported values [34, 40].

### C. EXAFS

To confirm the anti-site disorder between Fe and Ru atoms in FeRuCrSi, we have also carried out Extended X-ray Absorption Fine Structure (EXAFS) at Fe and Ru edges. Unlike XRD, EXAFS is an element-specific mea-

TABLE II. Bond length (R), coordination number (N), and Debye-Waller or disorder factor ( $\sigma^2$ ) obtained by simultaneous fitting of EXAFS data of FeRuCrSi at Fe and Ru edges.

Fe edge				Ru Edge			
Path	R ( $\text{\AA}$ )	N	$\sigma^2$	Path	R ( $\text{\AA}$ )	N	$\sigma^2$
Fe-Si	$2.48 \pm 0.03$	4	$0.0300 \pm 0.0055$	Ru-Si	$2.43 \pm 0.08$	4	$0.0062 \pm 0.0005$
Fe-Cr	$2.49 \pm 0.01$	4	$0.0089 \pm 0.0005$	Ru-Cr	$2.50 \pm 0.01$	4	$0.0072 \pm 0.0007$
Fe-Ru	$2.76 \pm 0.01$	3.5	$0.0089 \pm 0.0018$	Ru-Fe	$2.75 \pm 0.01$	3.3	$0.0085 \pm 0.0013$
Fe-Fe	$2.75 \pm 0.01$	2.5	$0.0018 \pm 0.0010$	Ru-Ru	$2.79 \pm 0.01$	2.7	$0.0092 \pm 0.0016$
Fe-Ru	$4.05 \pm 0.01$	6	$0.0300 \pm 0.0130$	Ru-Fe	$4.05 \pm 0.03$	6	$0.0190 \pm 0.0021$
Fe-Fe	$4.05 \pm 0.01$	6	$0.0160 \pm 0.0020$	Ru-Ru	$4.13 \pm 0.04$	6	$0.0175 \pm 0.0028$

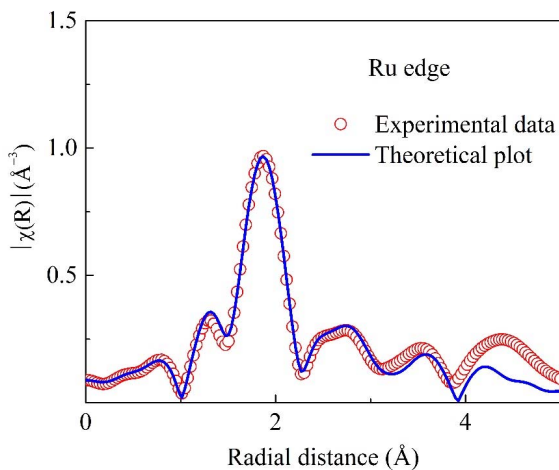
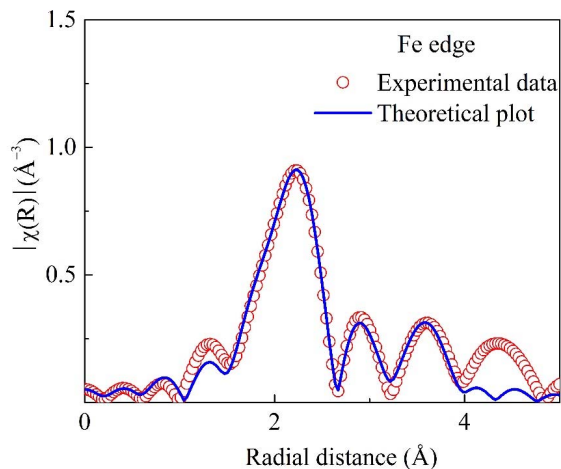


FIG. 5. Fourier transformed EXAFS spectra of FeRuCrSi taken at (a) Fe edge and (b) Ru edge.

surement that focuses on the local atomic environment surrounding the examined atoms. In the case of Heusler alloys, EXAFS has proven to be a valuable tool for elucidating precise atomic arrangements [13, 21, 51].

The normalized EXAFS ( $\mu(E)$  versus  $E$ ) spectra measured at the Fe and Ru edges are illustrated in Fig. 4. The standard procedure was followed in processing the

EXAFS data analysis [52]. In brief, the absorption spectra ( $\mu(E)$  vs.  $E$ ) were transformed into the absorption function  $\chi(E)$ , as given by eqn. 1, to obtain quantitative information on the local structure.

$$\chi(E) = \frac{\mu(E) - \mu_0(E)}{\Delta\mu_0(E_0)} \quad (1)$$

The energy-dependent absorption coefficient  $\chi(E)$  was then converted to the wave number-dependent absorption coefficient using eqn. 2:

$$K = \sqrt{\frac{2m(E - E_0)}{\hbar^2}} \quad (2)$$

To enhance oscillations at high  $k$ ,  $\chi(k)$  was weighted by  $k^2$ . The resulting  $\chi(k)k^2$  functions were Fourier-transformed in R space to produce  $\chi(R)$  versus R plots, representing actual distances from the center of the absorbing atom. The data reduction, including background reduction and Fourier transformation, were carried out utilizing the ATHENA subroutine within the Demeter software package [53]. The FeRuCrSi sample's Fourier-transformed EXAFS spectra at the Fe and Ru edges are presented in Fig. 5 as  $\chi(R)$  versus R plots.

The goodness of fit was assessed using the  $R_{factor}$  defined by Equation 3:

$$R_{factor} = \frac{[Im(\chi_{dat}(r_i) - \chi_{th}(r_i))]^2 + [Re(\chi_{dat}(r_i) - \chi_{th}(r_i))]^2}{[Im(\chi_{dat}(r_i))]^2 + [Re(\chi_{dat}(r_i))]^2} \quad (3)$$

Here,  $\chi_{dat}$  and  $\chi_{th}$  represent experimental and theoretical values, respectively, while  $Im$  and  $Re$  denote the imaginary and real parts, respectively. The ATOMS and ARTEMIS subroutines within the Demeter software package were employed for generating theoretical routes from crystallographic structures and fitting experimental data to theoretical simulations, respectively.

The simultaneous fitting of Fe and Ru edges could only be achieved under the assumption of disorder, confirming disorder in the examined compound based on the XRD data. The best-fit theoretical spectra and experimental data are presented in Fig. 5, and the corresponding parameters are listed in Table II. The EXAFS estimate a



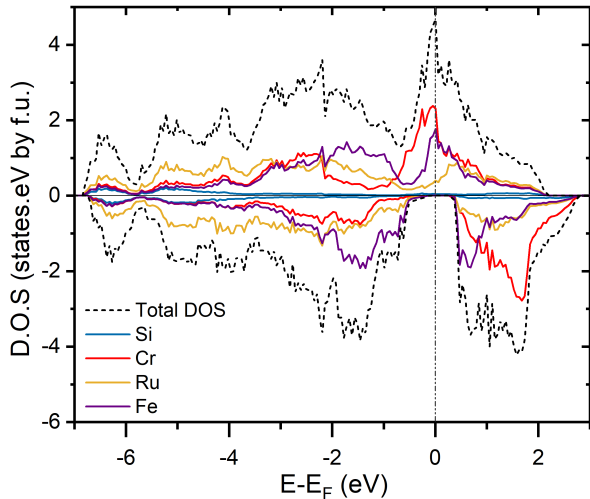


FIG. 6. Partial density of states for FeRuCrSi for disordered structure.

ratio of Fe/Ru mixing as 59:41 and 45:55, while measuring from Fe and Ru edges, respectively. The EXAFS data fitting aligns well with a disordered structure of Type-1, corroborating our XRD data analysis.

#### D. Electronic structure calculations for disordered crystal structure

Following our finding of a 50:50 site disorder between Fe and Ru atoms, we have extended the electronic structure calculations for FeRuCrSi considering the same disorder in the theoretical analysis (Fig. 6). Theoretical computations reveal that despite structural disorder, the system maintains 100% spin polarization. Additionally, the total magnetic moment estimated to be  $1.94 \mu_B$ , consistent with both the ordered structure and the Slater-Pauling value. Specifically, magnetic moments for individual sites in the disordered structure are estimated as follows: Si =  $-0.008 \mu_B$ , Cr =  $1.898 \mu_B$ , Ru =  $-0.161 \mu_B$ , and Fe =  $0.211 \mu_B$ .

#### E. Magnetic properties

Fig. 7 represents the magnetization *vs.* temperature of FeRuCrSi measured in both zero field cooled (ZFC) and field cooled (FC) condition under an application of 100 Oe field. Thermo-magnetic irreversibility observed between ZFC and FC magnetization which vanishes when the external field strength is enhanced to 500 Oe and beyond. The susceptibility shows a sharp ferromagnetic to paramagnetic transition near its Curie temperature,  $T_C = 217$  K, which is determined from the minima of  $d(M/H)/dT$  curve.

The isothermal magnetization measurements were also carried out below (4 K) and above (300 K) the Curie temperature (Fig. 8). The magnetic isotherm at 4 K ex-

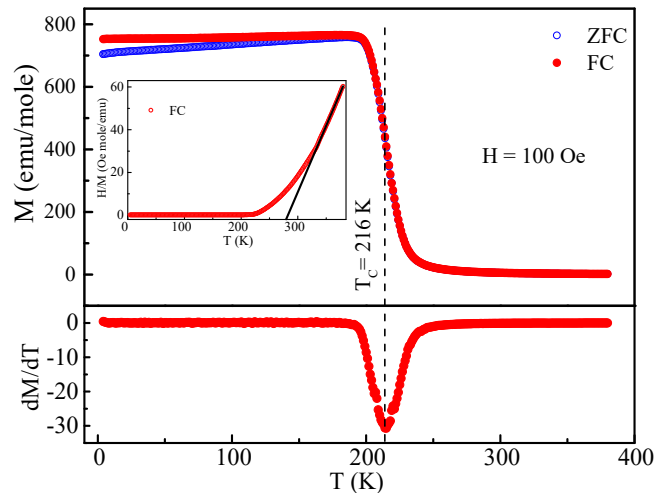


FIG. 7. Temperature dependence of magnetization in FeRuCrSi measured in 100 Oe applied magnetic field under ZFC (blue circle) and FC (red circle) conditions. Curie temperature,  $T_C$ , is determined from the minima in  $dM/dT$  *vs.*  $T$  plot. Inset shows inverse susceptibility data measured under FC condition. At high temperature region, Curie-Weiss fit with extrapolated section has also been shown.

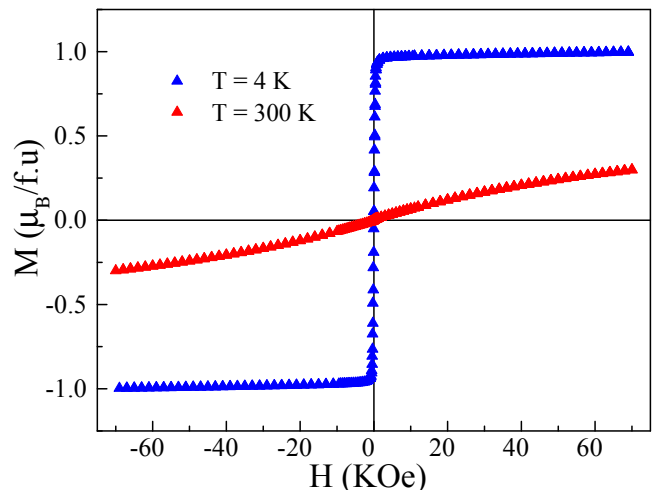


FIG. 8. Isothermal magnetization of FeRuCrSi measured at 4 K and 300 K.

hibit a soft ferromagnetic character with the saturation magnetic moment as  $0.97 \mu_B/f.u.$ , much smaller than  $2 \mu_B/f.u.$ , expected from the S-P rule described earlier (Sec. III A). Interestingly, although the Curie temperature in our system is 217 K, the magnetic isotherm at a much higher temperature, 300 K, exhibit a small but definite nonlinear character, suggesting possible presence of ferromagnetic interaction at such high temperature above  $T_C$ . The presence of ferromagnetic interaction, extending upto 300 K and even beyond, has also cast its signature in the magnetic susceptibility results as the inverse susceptibility deviates from linearity below 330 K (inset of Fig. 7). The linear character of inverse susceptibility is the hallmark of the paramagnetic system as suggested

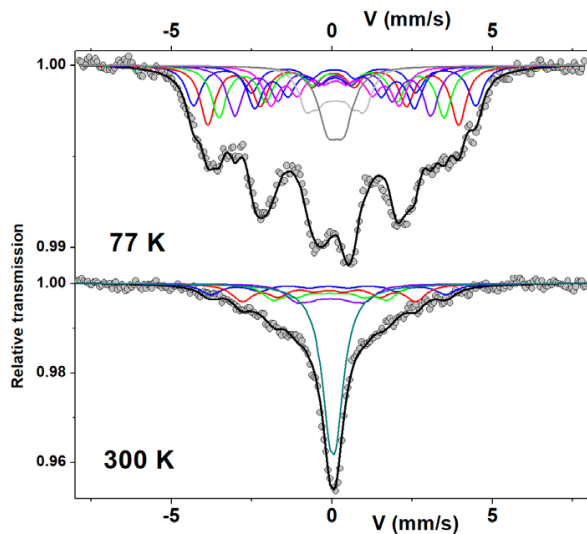


FIG. 9. Mössbauer spectra and the multi-component description (see text) of FeRuCrSi taken at 77 K (up) and 300 K (bottom).

by Curie-Weiss law, and its deviation from linearity below 330 K suggests the presence of ferromagnetic clusters persisting in the system at much higher temperature in comparison to its Curie temperature. It may be noted that in literature, a range of Curie temperature ( $T_C$ ) and saturation magnetic moment ( $M_{sat}$ ), from 346 K to 370 K, and  $1.27 \mu_B/\text{f.u.}$  to  $1.84 \mu_B/\text{f.u.}$ , respectively, have been reported by various groups while investigating the same composition [33, 40]. It is thus quite possible that variation of local disorder in those reported systems are responsible for such variation of  $T_C$  and  $M_{sat}$ . In our case, although the bulk  $T_C$  is  $\sim 217$  K, it is thus likely that random distribution of atomic disorder results some local regions having suitable conditions for higher  $T_C$  in isolated clusters.

#### F. Mössbauer spectrometry

To verify the existence of structural disorder and its influence on the magnetic properties of FeRuCrSi,  $^{57}\text{Fe}$  Mössbauer spectrometry was carried at 77 K and 300 K. The Mössbauer spectra for both temperatures reveal magnetic sextets superimposed on a central quadrupolar feature. The magnetic contribution very prominent in the spectrum at 77 K, whereas it is much weaker at 300 K. Given that our complete XRD and EXAFS analyses validate a 50:50 site distribution between Fe and Ru at the  $4c$  and  $4d$  positions, one would therefore expect the Mössbauer spectra only two magnetic sextets (associated with positions  $4c$  and  $4d$ ) well below the Curie temperature. However, the Mössbauer spectrum taken at 77 K cannot be adequately described with a simple 2 components model. To account physically for this complex hyperfine structure, a minimum of 8 components is

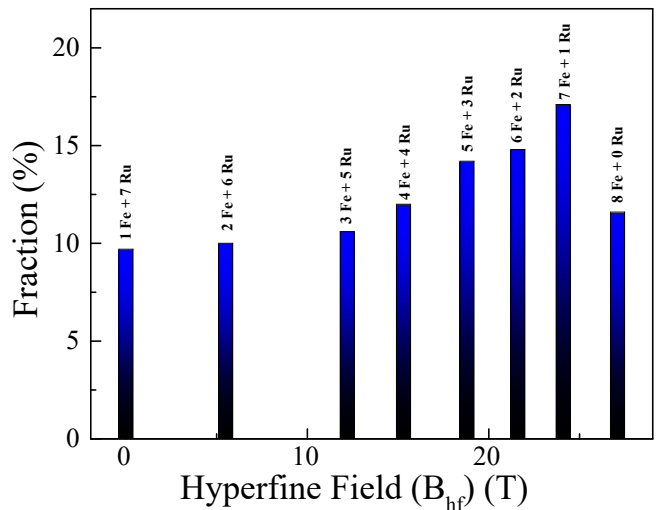


FIG. 10. Relative fraction as a function of hyperfine field for each distribution in disordered structure of FeRuCrSi. The description excludes the configuration where all the  $4c$  and  $4d$  positions are occupied by Ru atoms only.

required for a satisfactory fit, in agreement with the number of possible environments. The Mössbauer spectrum at 77 K (Fig. 9) is fitted with 7 magnetic sextets, all showing almost similar isomer shift values, and a quadrupolar component (see Table III), the line widths being fitted with the same value. The small variation of isomer shift could be taken as an indication of variations in the electron density at the Fe nuclei as a function of their atomic environments. The slightly larger isomer-shift align with the various possibilities of atomic environments sharing the same number for each species. In addition, the isomer shift follows a more or less regular increase as the hyperfine field decreases, which includes the quadrupolar component. Another possible description which can be obtained by considering a linear decrease of isomer shift correlated to decreasing hyperfine field values, leads to fairly similar conclusions.

The refined values of the hyperfine parameters are given in Table III. The average hyperfine field is thus estimated at 16.8 Tesla for such an 8-component fit comprising 7 different magnetic sextets. For the calibration of magnetic moment from hyperfine field values, usually  $\alpha\text{-Fe}$  with a magnetic moment of  $2 \mu_B$  producing a hyperfine field of 33 Tesla is considered as standard. So, for a 16.8 Tesla magnetic field, a moment of  $1.0 \mu_B$  is obtained, which matches very closely with the moment obtained from isothermal magnetization (Sec. III E). This is a very surprising result which states that Fe atoms are the primary source to the magnetic moment: indeed, this convincing result is completely inconsistent with all the DFT calculations reported [32, 33], as well as with the one presented in this work (Sec. III A) which predicts that Cr should be the major source to the magnetic moment, while the magnetic moment at the Fe site would be induced in nature. This is also one of the main reasons why the isothermal saturation magnetization values

TABLE III. Refined values of hyperfine parameters for Mössbauer spectra measured at 77 K and 300 K in the FeRuCrSi Heusler alloy. Isomer shift ( $\delta$ ) (quoted relative to  $\alpha$ -Fe at 300 K), quadrupolar splitting ( $\Delta$ ), quadrupolar shift ( $2\varepsilon$ ), hyperfine field ( $B_{hf}$ ) and relative absorption areas (RA).

T (K)	$\delta$ (mm/s)	$\Delta$ or $2\varepsilon$ (mm/s)	$B_{hf}$ (T)	Distribution	RA
	$\pm 0.01$	$\pm 0.01$	$\pm 0.5$		$\pm 1$
	0.21	0.03	27.1	8 Fe + 0 Ru	12
	0.18	0	24.1	7 Fe + 1 Ru	17
	0.12	0	21.6	6 Fe + 2 Ru	15
	0.20	-0.07	18.8	5 Fe + 3 Ru	14
77	0.22	0	15.3	4 Fe + 4 Ru	12
	0.23	0	12.2	3 Fe + 5 Ru	11
	0.24	0	5.5	2 Fe + 6 Ru	10
	0.26	0.45	-	1 Fe + 7 Ru	9
	0.025	0	22.6	8 Fe + 0 Ru	11
	0.04	0	16.6	7 Fe + 1 Ru	18
300	0.08	0	10.9	6 Fe + 2 Ru	15
	0.10	0	6.6	5 Fe + 3 Ru	14
	0.155	0	-		42

for this compound deviate from those proposed by the DFT calculations. This also explain why with increasing Fe concentration, the saturation magnetic moment and  $T_C$  in  $\text{Ru}_{2-x}\text{Fe}_x\text{CrSi}$  have been reported to increase linearly [40] and not remain constant to  $2 \mu_B/\text{f.u.}$  Fe being the major contributor of magnetic moment in this series also explain why this compound experimentally deviates from the theoretically predicted HMF character.

It is interesting to note, as discussed above, tha the  $^{57}\text{Fe}$  Mössbauer spectra could only be analysed by considering 8 different components corresponding to 8 different Fe environments, whereas the XRD and EXAFS measurements suggest that Fe atoms are randomly distributed along Ru atoms only in two crystallographic sites, i.e.  $4c$  and  $4d$ . This apparent contradiction can be easily understood if we consider that the random distribution of Fe atoms resulting from a large number of different localised atomic environments. When Fe is randomly distributed between  $4c$  and  $4d$  sites, there can be 9 different possibilities of atomic distributions, ranging from all 8 atoms being Fe in some unit cells, all 8 Ru in other unit cells, and the rest of the unit cells has varying degree of mixing with the restriction that when averaged over all unit cells, the composition remains FeRuCrSi. These 9 possibilities are: 8 Fe + 0 Ru, 7 Fe + 1 Ru, 6 Fe + 2 Ru, 5 Fe + 3 Ru, 4 Fe + 4 Ru, 3 Fe + 5 Ru, 2 Fe + 6 Ru, 7 Fe + 1 Ru, 0 Fe + 8 Ru. Since  $^{57}\text{Fe}$  Mössbauer measurements can only detect Fe atoms, the configuration involving 0 Fe + 8 Ru would not be related to the Mössbauer results, but would provide a very useful nature about the 8 remaining configurations.

As it has been previously mentioned that  $\text{Fe}_2\text{CrSi}$  exhibits a ferromagnetic ordering at 520 K [35], while all other members of the Ru-diluted  $\text{Ru}_{2-x}\text{Fe}_x\text{CrSi}$  series possess a lower Curie temperature [30, 41], an attempt can be made to correlate the reduction of  $T_C$  in this se-

ries with a reduced magnetic interaction strength caused by non-magnetic (Ru) dilution of the local atomic environment of Fe. Using the same logic in our system, we correlated the different hyperfine magnetic field values of the 8 components of the Mössbauer spectra at 77 K with 8 different atomic environments of the Fe atoms. The largest hyperfine field is shown by the Fe atoms in the unit cell that has only Fe atoms in all the  $4c$  and  $4d$  positions, while the single quadrupolar component which shows no hyperfine field has only 1 Fe atom together with 7 Ru atoms in the unit cell. Excluding the 0 Fe + 8 Ru configuration, our Mössbauer analysis suggests that all the other 8 configurations are present in our system with almost equal probabilities (Table III). The average value of the magnetic hyperfine field represents the average magnetic interaction which in turn determines the bulk saturation moment as well as  $T_C$ . This is also corroborated from our Mössbauer spectrum taken at 300 K, where the first four components presented in Table III still show weak hyperfine fields, although the bulk  $T_C$  of our sample, as determined from magnetic susceptibility measurements, is much lower ( $\sim 217$  K). The non-linearity of the inverse susceptibility (Fig. 7) below  $\sim 330$  K is probably caused by the presence of such magnetic clusters in our system. The different distribution of the local atomic environment may also explain the variation in  $M_{sat}$  and  $T_C$  reported by various groups for the same equiatomic quaternary Heusler alloy FeRuCrSi. The presence of larger fractions of configurations with more Fe magnetic moments would lead to larger  $M_{sat}$  and  $T_C$  and vice versa. Our results therefore establish a rather rare and complex scenario in which the main physical properties are strongly correlated to the material chemistry in the form of random atomic disorder on a localised scale. This level of understanding of atomic arrangement using Mössbauer spectrometry is remark-



able and echoes previous studies based on another related technique, namely nuclear magnetic resonance measurements in other Heusler alloys [12, 54, 55].

### G. Conclusion

In conclusion, in this work we have used X-ray diffraction, extended X-ray absorption fine structure,  $^{57}\text{Fe}$  Mössbauer spectrometry and magnetic measurements in a quaternary Heusler alloy,  $\text{FeRuCrSi}$ , belonging to  $\text{Ru}_{2-x}\text{Fe}_x\text{CrSi}$  series. Since DFT calculations indicate that Cr is a moment carrying atom, all theoretical calculations predict a saturation magnetic moment of  $2 \mu_B/\text{f.u.}$  with robust half-metallicity with 100% spin polarisation for all Fe containing members of this series. However, even for the same composition, there are reports with large variation in Curie temperatures and saturation moments which often deviate significantly from theoretical predictions. Based on our comprehensive

structural analysis, we have discovered that the magnetic moment in this system actually comes from Fe atoms, not Cr. The dominant role of Fe in the magnetism explains the experimental deviations from the theoretical predictions and highlights the influence of local atomic disorder on the physical properties. This study highlights the complex relationship between the chemistry of the material, atomic disorder, and the physical properties of the  $\text{Ru}_{2-x}\text{Fe}_x\text{CrSi}$  series.

### Acknowledgement

S.G and S.C would like to sincerely acknowledge SINP, India and UGC, India, respectively, for their fellowship. DFT calculations were performed using HPC resources from GENCI-CINES (Grant 2021-A0100906175). Part of this work was performed under CSRP project 6908-3 of the Indo-French Centre for Promotion of Advanced Research, New Delhi, India.

- 
- [1] D. D. Awschalom and M. E. Flatté, *Nature physics* **3**, 153 (2007).
- [2] I. Žutić, J. Fabian, and S. D. Sarma, *Reviews of modern physics* **76**, 323 (2004).
- [3] F. Pulizzi, *Nature materials* **11**, 367 (2012).
- [4] C. Felser, G. H. Fecher, and B. Balke, *Angew. Chem. Int. Ed.* **46**, 668 (2007).
- [5] R. A. De Groot, F. M. Mueller, P. G. Van Engen, and K. H. J. Buschow, *Phys. Rev. Lett.* **50**, 2024 (1983).
- [6] X. L. Wang, *Physical review letters* **100**, 156404 (2008).
- [7] Ikhtiar, S. Kasai, A. Itoh, Y. Takahashi, T. Ohkubo, S. Mitani, and K. Hono, *Journal of Applied Physics* **115**, 173912 (2014).
- [8] T. Saito, N. Tezuka, M. Matsuura, and S. Sugimoto, *Applied Physics Express* **6**, 103006 (2013).
- [9] T. Kubota, S. Tsunegi, M. Oogane, S. Mizukami, T. Miyazaki, H. Naganuma, and Y. Ando, *Applied Physics Letters* **94**, 122504 (2009).
- [10] V. Alijani, J. Winterlik, G. H. Fecher, S. S. Naghavi, and C. Felser, *Phys. Rev. B* **83**, 184428 (2011).
- [11] V. Alijani, S. Ouardi, G. H. Fecher, J. Winterlik, S. S. Naghavi, X. Kozina, G. Stryganyuk, C. Felser, E. Ikenaga, Y. Yamashita, *et al.*, *Phys. Rev. B* **84**, 224416 (2011).
- [12] S. Gupta, S. Chakraborty, S. Pakhira, C. Barreateau, J.-C. Crivello, B. Bandyopadhyay, J. M. Greneche, E. Alleno, and C. Mazumdar, *Phys. Rev. B* **106**, 115148 (2022).
- [13] S. Gupta, S. Chakraborty, V. Bhasin, S. Pakhira, S. Dan, C. Barreateau, J.-C. Crivello, S. N. Jha, M. Avdeev, J.-M. Greneche, D. Bhattacharyya, E. Alleno, and C. Mazumdar, *Phys. Rev. B* **108**, 045137 (2023).
- [14] S. Gupta, S. Chakraborty, V. Bhasin, S. Pakhira, S. Dan, C. Barreateau, J.-C. Crivello, S. Jha, M. Avdeev, D. Bhattacharyya, *et al.*, *Journal of Materials Chemistry C* **11**, 15489 (2023).
- [15] L. Bainsla, A. Mallick, M. M. Raja, A. Nigam, B. C. S. Varaprasad, Y. Takahashi, A. Alam, K. Suresh, and K. Hono, *Phys. Rev. B* **91**, 104408 (2015).
- [16] L. Bainsla, A. Mallick, M. M. Raja, A. Coelho, A. Nigam, D. D. Johnson, A. Alam, and K. Suresh, *Phys. Rev. B* **92**, 045201 (2015).
- [17] S. Gupta, J. Sau, M. Kumar, and C. Mazumdar, *J. Mater. Chem. C* **12**, 706 (2024).
- [18] Y. Venkateswara, S. S. Samatham, P. Babu, K. Suresh, and A. Alam, *Physical Review B* **100**, 180404 (2019).
- [19] Y. Venkateswara, J. Nag, S. S. Samatham, A. K. Patel, P. Babu, M. R. Varma, J. Nayak, K. Suresh, and A. Alam, *Physical Review B* **107**, L100401 (2023).
- [20] S. Gupta, S. Chakraborty, S. Pakhira, A. Biswas, Y. Mudryk, A. Kumar, B. Mukherjee, G. S. Okram, A. Das, V. K. Pecharsky, *et al.*, *Phys. Rev. B* **107**, 184408 (2023).
- [21] S. Gupta, S. Chakraborty, V. Bhasin, S. Pakhira, A. Biswas, Y. Mudryk, A. Kumar, C. Barreateau, J.-C. Crivello, A. Das, S. N. Jha, D. Bhattacharyya, V. K. Pecharsky, E. Alleno, and C. Mazumdar, *Phys. Rev. B* **108**, 054405 (2023).
- [22] J. Nag, D. Rani, J. Kangsabanik, D. Singh, R. Venkatesh, P. Babu, K. Suresh, and A. Alam, *Physical Review B* **104**, 134406 (2021).
- [23] G. Xu, E. Liu, Y. Du, G. Li, G. Liu, W. Wang, and G. Wu, *Europhysics Letters* **102**, 17007 (2013).
- [24] Q. Gao, I. Opahle, and H. Zhang, *Physical Review Materials* **3**, 024410 (2019).
- [25] S. Skaftouros, K. Özdoğan, E. Şaşıoğlu, and I. Galanakis, *Applied physics letters* **102** (2013).
- [26] Q. Gao, H.-H. Xie, L. Li, G. Lei, J.-B. Deng, and X.-R. Hu, *Superlattices and Microstructures* **85**, 536 (2015).
- [27] S. Ouardi, G. H. Fecher, C. Felser, and J. Kübler, *Physical review letters* **110**, 100401 (2013).
- [28] Y. Venkateswara, S. Gupta, S. S. Samatham, M. R. Varma, K. Suresh, A. Alam, *et al.*, *Physical Review B* **97**, 054407 (2018).
- [29] S. Mizutani, S. Ishida, S. Fujii, and S. Asano, *Materials transactions* **47**, 25 (2006).
- [30] M. Hiroi, T. Rokkaku, S. Mizutani, S. Fujii, and S. Ishida, in *Journal of Physics: Conference Series*, Vol. 150 (IOP Publishing, 2009) p. 042058.

- [31] M. Hiroi, T. Rokkaku, K. Matsuda, T. Hisamatsu, I. Shigeta, M. Ito, T. Sakon, K. Koyama, K. Watanabe, S. Nakamura, *et al.*, *Physical Review B* **79**, 224423 (2009).
- [32] X. Guo, Z. Ni, Z. Liang, and H. Luo, *Computational Materials Science* **154**, 442 (2018).
- [33] G. Zhang, H. Hao, Y. Liang, Y. Qiao, S. Bai, H. Liu, and H. Luo, *Journal of Physics and Chemistry of Solids* **181**, 111541 (2023).
- [34] X. Wang, H. Khachai, R. Khenata, H. Yuan, L. Wang, W. Wang, A. Bouhemadou, L. Hao, X. Dai, R. Guo, *et al.*, *Scientific reports* **7**, 16183 (2017).
- [35] H. Luo, Z. Zhu, L. Ma, S. Xu, H. Liu, J. Qu, Y. Li, and G. Wu, *Journal of Physics D: Applied Physics* **40**, 7121 (2007).
- [36] M. Hiroi, K. Uchida, I. Shigeta, M. Ito, K. Koyama, S. Kimura, and K. Watanabe, *Journal of the Korean Physical Society* **62**, 2068 (2013).
- [37] I. Galanakis, P. Dederichs, and N. Papanikolaou, *Phys. Rev. B* **66**, 174429 (2002).
- [38] K. Özdoğan, E. Şaşıoğlu, and I. Galanakis, *J. Appl. Phys.* **113**, 193903 (2013).
- [39] S. Bahlouli, Z. Aarizou, and M. Elchikh, *Modern Physics Letters B* **27**, 1350219 (2013).
- [40] K. Matsuda, M. Hiroi, and M. Kawakami, *Journal of Physics: Condensed Matter* **17**, 5889 (2005).
- [41] M. Hiroi, S. Nishiinoue, I. Shigeta, M. Ito, K. Koyama, A. Kondo, K. Kindo, I. Watanabe, M. Fujii, S. Kimura, *et al.*, *Physical Review B* **103**, 094428 (2021).
- [42] M. Hiroi, T. Hisamatsu, T. Suzuki, K. Ohishi, Y. Ishii, and I. Watanabe, *Physical Review B* **88**, 024409 (2013).
- [43] M. Ito, T. Hisamatsu, T. Rokkaku, I. Shigeta, H. Manaka, N. Terada, and M. Hiroi, *Physical Review B* **82**, 024406 (2010).
- [44] J. Rodríguez-Carvajal, *Phys. B: Condens. Matter* **192**, 55 (1993).
- [45] P. E. Blöchl, *Physical Review B* **50**, 17953 (1994).
- [46] G. Kresse and J. Hafner, *Physical Review B* **48**, 13115 (1993).
- [47] G. Kresse and J. Hafner, *Journal of Physics: Condensed Matter* **6**, 8245 (1994).
- [48] B. K. Perdew, J. P. and M. Ernzerhof, *Physical Review Letters* **77**, 3865 (1996).
- [49] I. Galanakis, P. Mavropoulos, and P. H. Dederichs, *Journal of Physics D: Applied Physics* **39**, 765 (2006).
- [50] Y. Venkateswara, D. Rani, K. Suresh, and A. Alam, *J. Magn. Magn* **502**, 166536 (2020).
- [51] B. Balke, S. Wurmehl, G. H. Fecher, C. Felser, M. C. Alves, F. Bernardi, and J. Morais, *Appl. Phys. Lett.* **90**, 172501 (2007).
- [52] D. C. Koningsberger and R. Prins, (1987).
- [53] B. Ravel and M. Newville, *J. Synchrotron Radiat.* **12**, 537 (2005).
- [54] S. Wurmehl, A. Alfonsov, J. Kohlhepp, H. Swagten, B. Koopmans, M. Wójcik, B. Balke, V. Ksenofontov, C. Blum, and B. Büchner, *Physical Review B* **88**, 134424 (2013).
- [55] S. Wurmehl, J. T. Kohlhepp, H. J. Swagten, B. Koopmans, M. Wójcik, B. Balke, C. G. Blum, V. Ksenofontov, G. H. Fecher, and C. Felser, *Applied Physics Letters* **91** (2007).